Carbon Letters (2021) 31:1237–1248
https://doi.org/10.1007/s42823-021-00247-0

Online ISSN 2233-4998
Print ISSN 1976-4251

ORIGINAL ARTICLE

An investigation on development of a molecular imprinted sensor with graphitic carbon nitride (g-C_3N_4) quantum dots for detection of acetaminophen

Hilal Medetalibeyoğlu[1]

Received: 14 November 2020 / Revised: 17 March 2021 / Accepted: 23 March 2021 / Published online: 8 April 2021

Abstract
In the present study, a novel electrochemical sensor for acetaminophen (AMP) which included quantum graphitic carbon nitride dots, g-C_3N_4QDs, was designed and conducted with molecular imprinted polymer (MIP). First, bulk g-C_3N_4 was generated with direct thermal polycondensation of melamine. After the treatment of the acidic solution containing H_2SO_4: HNO_3 (1:1, v:v), the heating treatment at 200 °C on the dispersion provided g-C_3N_4QDs. In this respect, for nanomaterial characterization, some spectroscopic approaches were performed including Fourier-transform infrared spectroscopy (FT-IR), and X-ray photoelectron spectroscopy (XPS) as well as electroanalytical methods such as electrochemical impedance (EIS) and cyclic voltammetry (CV). In accordance with the aims of the study, AMP imprinted electrode was formed after high electrocatalytic performance and linear range of 1.0×10^{-11}–2.0×10^{-8} M and the LODs of 2.0×10^{-12} was achieved. Eventually, an AMP-printed sensor was also used for AMP identification in pharmaceutical samples.

Keywords Molecular imprinted sensor · Acetaminophen · Pharmaceutical sample · Graphitic carbon nitride quantum dots

1 Introduction

Pharmaceutical contaminants have led to great concern as a result of their impact on public health. A number of pharmaceutical compounds have adverse effects on health, one of which involves hepatic failure [1]. AMP is one of the antipyretic drugs known as "Paracetamol" [2]. Such chemical agents contaminate an aquatic environment because of being easily accessible. Efficient methods are, therefore, required to determine these pharmaceutical agents.

Up to date, AMP detection has been documented on liquid chromatography [3], spectrophotometry [4], chemiluminescence [5], and electrochemistry [6]. However, for sensitive applications, difficult sample pretreatment and costly instruments are required, which issues make it extremely necessary for sensor development using responsive, cost-effective, and efficient methods such as electrochemistry. Furthermore, MIP-based electrochemical methods for the selective recognition of pharmaceuticals, toxic substances, and biomolecules have often been used due to their mechanical properties and their low cost [7, 8]. Modified electrodes currently have strong sensor applications to trace detection applications on drugs or other ambient samples including organic substrates, molecular imprinted polymers, nanomaterials, and nanocomposites because of their high sensitiveness, the catalytic effect, and low toxicity [9–22]. In this research, the modified electrode has been developed to boost the electrochemical catalytic performance through a molecular imprinted sensor, including graphitic carbon nitride (g-C_3N_4). In this respect, g-C_3N_4 attention for development of sensors [9, 10]. The interaction of van der Waals among g-C_3N_4 layers provides chemical stability in solvents including water and *o*-dichlorobenzene. However, because of the low cost, heat stability, high area (2500 $m^2\ g^{-1}$), and feasibility in surface engineering, g-C_3N_4 is commonly used as a catalyst [23–33]. In literature, graphitic carbon nitride-based electrochemical sensors were presented. First, molecular imprinted voltammetric sensor based on carbon nitride nanotubes was prepared for determination of melamine and the detection limit was calculated as 1.0×10^{-11} M [34]. Second, carbon nitride nanotubes decorated with graphene quantum dots for electrochemical determination of

✉ Hilal Medetalibeyoğlu
hilalmedet@gmail.com

[1] Faculty of Science and Letters, Department of Chemistry, Kafkas University, Kars, Turkey

chlorpyrifos was developed and the linearity range was obtained as 1.0×10^{-11}–1.0×10^{-9} M [35]. Finally, the molecular imprinting polymer with polyoxometalate/carbon nitride nanotubes for electrochemical recognition of bilirubin was presented and the detection limit was calculated as 3.0×10^{-13} M [36]. Based upon the findings in the literature, a molecular imprinted sensor like g-C_3N_4QDs was not identified for the electrochemical catalytic performance of acetaminophen. In this research, the sensor produced is realized to have a high catalytic electrochemical effect and is simple and ecological.

2 Experimental

2.1 Materials

AMP, aminocaproic acid (AA), D-phenylalanine (DPA), L-phenylalanine (LPA), L-L-arginine (LA), ascorbic acid (LAA), glucose (GLU), pyrrole, and melamine were bought from Merck (Germany). As an electrolyte and dilution buffer, the phosphate buffer (pH 7.5, PBS, 0.1 M) was used.

2.2 Preparation of bulk g-C_3N_4 and g-C_3N_4QDs

Bulk g-C_3N_4 was generated with direct thermal polycondensation of melamine based upon the literature [34]. The acidic solution containing H_2SO_4: HNO_3 (1:1, v:v) was administered 100.0 mg of bulk g-C_3N_4 for 10 h under ultrasound. The colloidal suspension was filtered with a microporous membrane after the solution had been diluted with ultrapurified water quality. The final product was distributed for 1 h under ultrasound in o-dichlorobenzenes (15 mL). In the Teflon-line autoclave, the dispersion was eventually heated at 200 °C for 15 h. The yellow solution g-C_3N_4QDs were obtained following the cooling process [37].

2.3 Preparation of electrode

In this investigation, the working glassy carbon electrodes (GCE) including g-C_3N_4/GCE and g-C_3N_4QDs/GCE were generated through reports by Yokuş et al. [38]. Eventually, 15µL (g-C_3N_4 and g-C_3N_4QDs) of the dispersion were lowered on the GCE surface, and the solution under an infrared lamp was evaporated.

2.4 Preparation of AMP imprinted electrodes

The AMP imprinted electrode preparation procedure (MIP/g-C_3N_4QDs/GCE) was introduced on Scheme 1. Furthermore, the other imprinted electrodes were prepared based on the literature [36].

Every imprinted electrode (MIP/GCE, MIP/g-C_3N_4/GCE, MIP/g-C_3N_4QDs/GCE) was grown in one blend of 100.0 mM pyrrole comprising of 25,0 mM AMP in 0,1 M PBS (pH 7.5) through CV for 20 cycles. Imprinted electrodes based on g-C_3N_4QDs without AMP (NIP/g-C_3N_4QDs/GCE) through CV were examined tin terms of the selectivity of imprinting. To break the electrostatic interactions between AMP and pyrrole, 1.0 M NaCl was used as a desorption solution. 1.0 M NaCl was used as desorption agent to break electrostatic interactions between acetaminophen and pyrrole. AMP electrodes imprinted in bathrooms (50 ml, 1.0 M NaCl, 250 rpm) were then swung at 25 °C. After 15 min, nitrogen gas was used so as to dry MIP/g-C_3N_4/GCE and MIP/g-C_3N_4QDs/GCE [39]. No pressure fluctuations were stored in both MIP and NIP electrodes. In addition, voltammograms were supplied in an isolation case without pressure fluctuations affecting sensor sensitivity.

2.5 Sample preparation

AMP pharmaceutical tablets were planned in reference to literature [40]. The pharmaceutical tablets contained AMP that was weighed and crushed in a mortar. The equivalent amount contained one tablet that was moved to a flask of 100 mL. Subsequently, 0.1 M PBS (50 mL, pH 7.5) was added and sonified to dissolve for 25 min. The working solutions were achieved through dilution of 0,1 M PBS from the supernatant.

3 Results and discussion

3.1 Characterization results

Figure 1a displays a TEM (transmission electron microscopy) image of the bulk g-C_3N_4, which illustrates its sheet-like and bulk structure. Its large size was over 1 µm as indicated in Fig. 1b. The bulk g-C_3N_4 was converted to g-C_3N_4QDs successfully following o-dichlorobenzene treatment under ultrasonication. g-C_3N_4QDs had size diameters of 5–10 nm. The reason why this approach is adapted involving the solvothermal treatment, is to supply good dispersibility in o-dichlorobenzene. Furthermore, images of MIP and NIP surfaces were obtained by scanning electron microscopy (SEM) (Fig. 1c, d). The MIP surface was fitted with a large polymer layer with a porous structure (Fig. 1c). When Fig. 1d is considered, the polymer layer on the nip surface with a smooth structure was noticeable. the porous and selective structure for the recognition of amp by means of molecular imprinting technique was therefore successfully prepared.

The chemical structures of the bulk g-C_3N_4 and g-C_3N_4QDs were characterized through FTIR

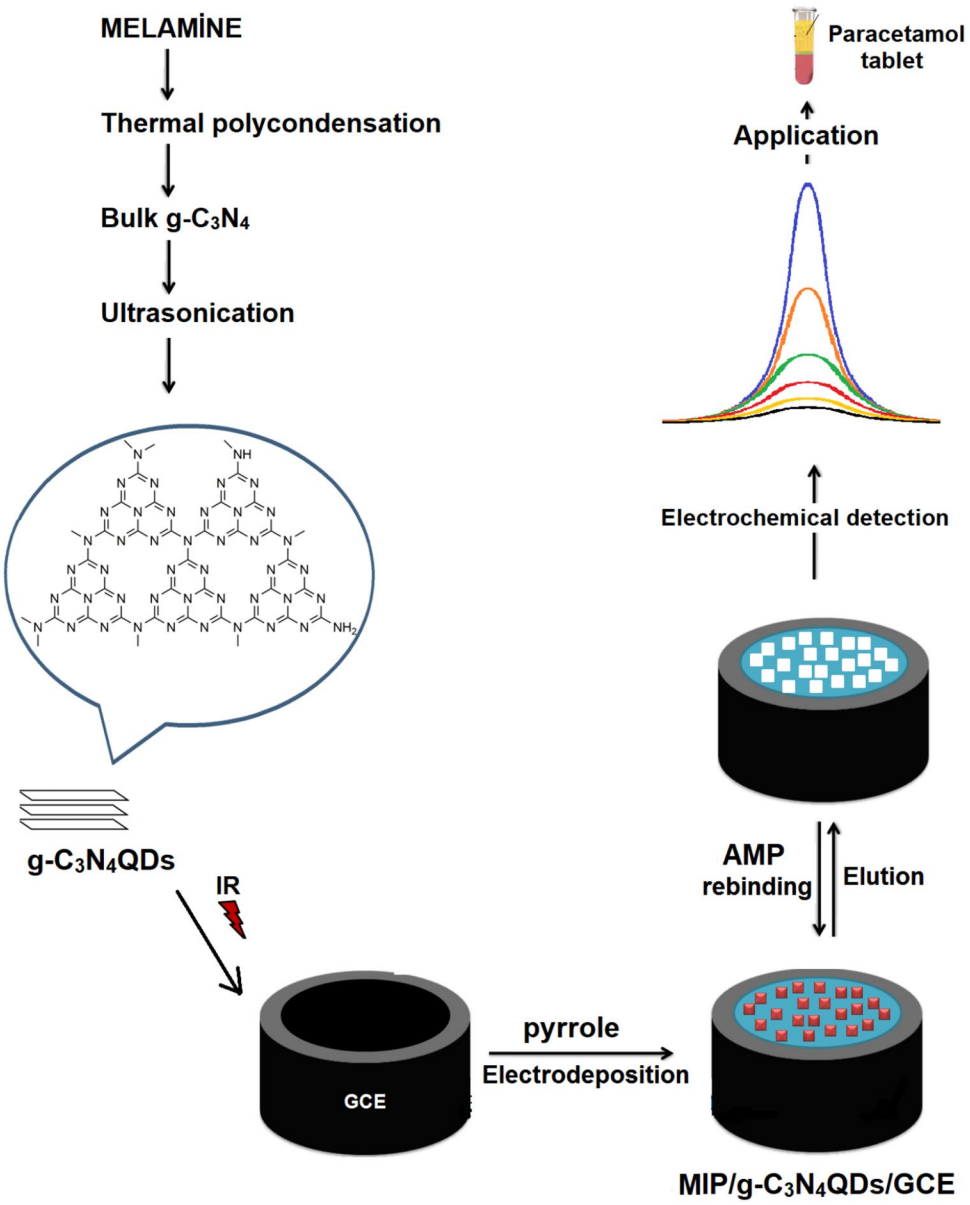

Scheme 1 Preparation procedure of AMP imprinted electrode

spectroscopy (Fig. 2). The vibrational bands at 1260, 1460, and 1640 cm^{-1} were corresponding to the usual stretching modes of CN heterocycles; the band at 803 cm^{-1} was corresponding to a triazine moiety on the spectrum of bulk g-C_3N_4 [41]. Similarly, these vibrational bands on the g-C_3N_4 bulk spectra were reported with the spectrum of g-C_3N_4QDs. Therefore, it can be suggested that the triazine units remained on the structure of the C_3N_4QDs throughout conversion of bulk g-C_3N_4 into g-C_3N_4QDs. The novel vibrational bands of 1380 and 1730 cm^{-1} were observed on the g-C_3N_4QDs spectra when the g-C_3N_4QDs spectra was analyzed. The bands at 1730 and 1380 cm^{-1} were C=O and C–O on the carboxylate group, respectively. The bands at 2845, 2910, and 2965 cm^{-1} were matched to the CHx stretching vibrations group [37], which indicated the presence of carboxylate and CHx groups during acidic treatment [42]. The formation of bulk g-C_3N_4 and g-C_3N_4QDs was verified through XPS. The C1s bands of bulk g-C_3N_4 at 284.1 and 288.5 eV were C–N–C, C–C, and C–$(N)_3$ bonds, respectively. The N1s bands at 398.6, 400.3, and 401.4 eV were C–N–C, N–$(C)_3$, and N–H, respectively (Fig. 3a) [43]. The C1s bands of g-C_3N_4QDs at 284.1, 285.5, and 288.5 eV were C–N–C, C–C, C–H, C=O, and C–$(N)_3$ bonds, respectively. During acidic treatment of bulk g-C_3N_4, C=O bands verified the formation of the carboxylate groups. Furthermore, the existence of carboxylate groups was confirmed by O1′s spectral analysis (C=O, C–OH). The N1s bands of g-C_3N_4QDs at 398.4, 400.5, and 401.6 eV were C–N–C, N–$(C)_3$, and N–H, respectively (Fig. 3b).

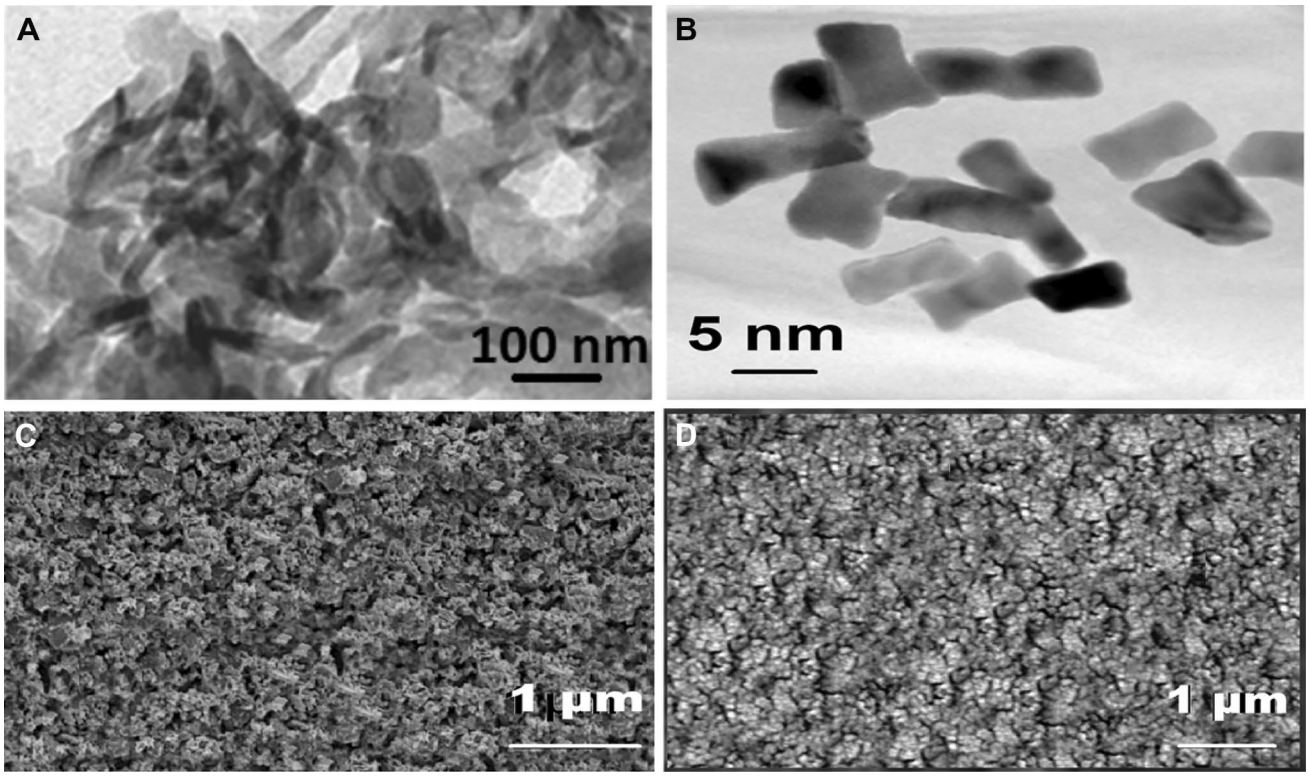

Fig. 1 TEM images of **a** bulk g-C_3N_4, **b** g-C_3N_4QDs and SEM images of **c** MIP/g-C_3N_4QDs/GCE, **d** NIP/g-C_3N_4QDs/GCE

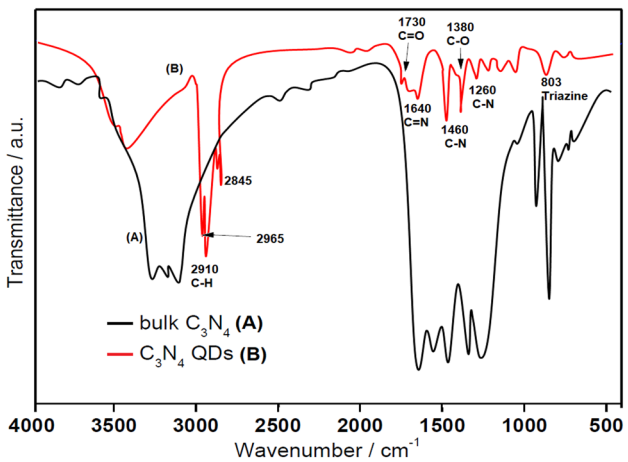

Fig. 2 FTIR spectra of bulk g-C_3N_4 and g-C_3N_4QDs

3.2 CV and EIS results

On bare GCE, the reversible peaks with 220 mV peak potential difference (ΔEp) were observed (curve of Fig. 4A). The more certain bands were found through use of g-C_3N_4/GCE (curve b of Fig. 4A) [44]. Because of its electrochemical active region (curve c of Fig. 4A), the lower mass transfer resistance was achieved using g-C_3N_4QDs/GCE (ΔEp = 100 mV). In bare GCE, g-C_3N_4/GCE and g-C_3N_4QDs/GCE electrochemical active areas were determined as 0.170 cm^2, 0.353 cm^2, and 0.849 cm^2, respectively, via the equation (Randles–Sevcik) of $i_p = 2.69 \times 10^5\ A\ n^{3/2}\ D^{1/2}\ C\ v^{1/2}$ [39]. Furthermore, various modified electrodes were obtained through EIS spectra (Fig. 4B). The values of charge transfer resistance (Rct) were 160 Ω (curve c), 120 Ω (curve b), and 80 Ω (curve a), respectively. Furthermore, the optimal sensor replies were obtained via g-C_3N_4QDs/GCE based on CV and EIS experiments.

3.3 Formation of AMP imprinted polymer on g-C_3N_4QDs/GCE

According to Fig. 4C, with a mixture of pyrrole containing an AMP molecule, the irreversible peaks decreased steadily with a scan at around + 0.72 V. The irreversible peaks of g-C_3N_4QDs/GCE were realized to disappear following the formation of adequate polymer layers on the electrode surface at 20th cycle. Figure 4D shows EIS of g-C_3N_4QDs/GCE (curve a), MIP/g-C_3N_4QDs/GCE without elution (curve c) and MIP/g-C_3N_4QDs/GCE after the removing of AMP (curve b) in 1.0 mM $[Fe(CN)_6]^{3-}$ containing 0.1 M KCl. After an electrochemical imprinted film was electrodeposited on g-C_3N_4QDs/GCE, the semicircle diameter increased. This case was assigned to covering of pyrrole. When AMP

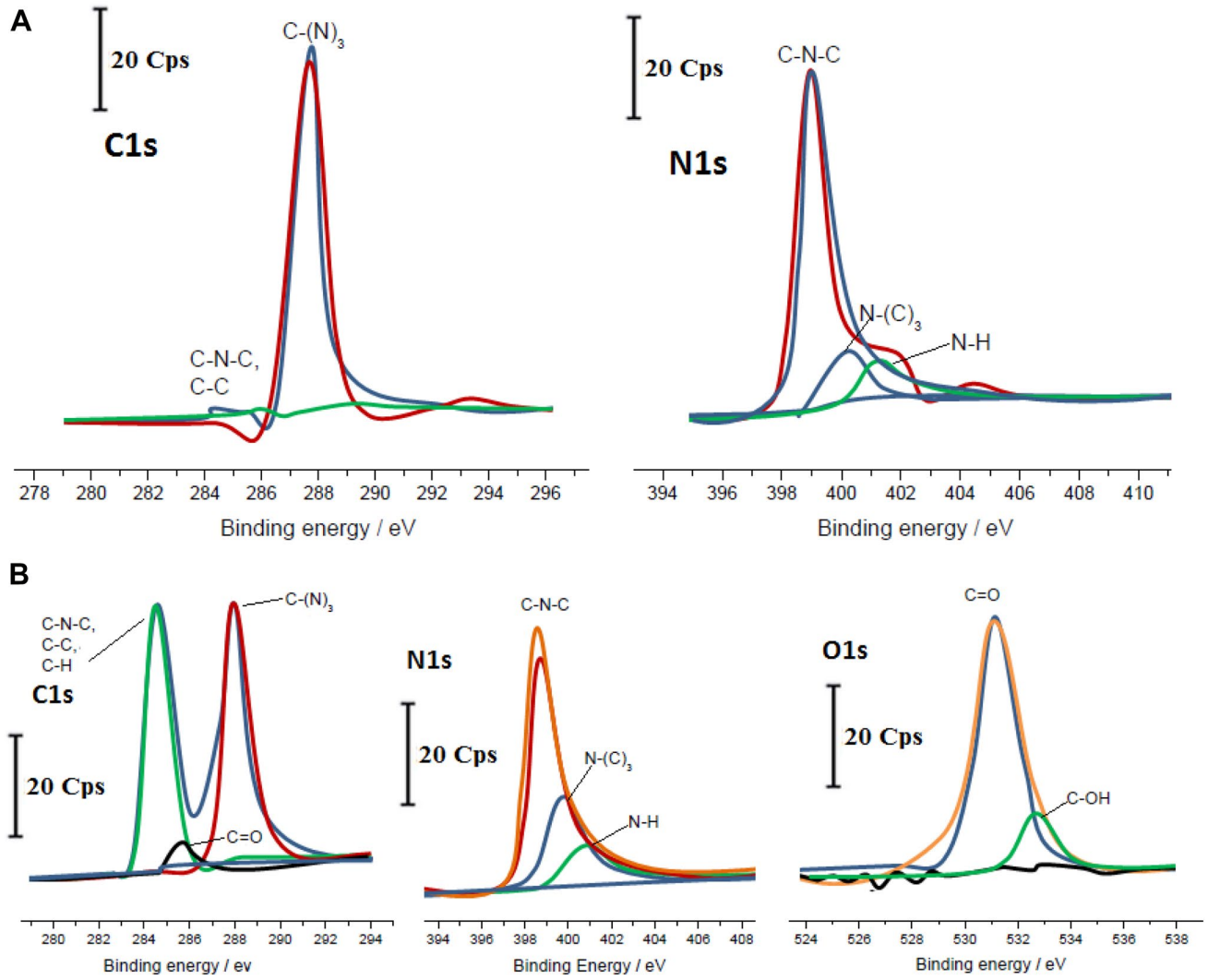

Fig. 3 XPS spectra of **a** bulk g-C_3N_4 and **b** g-C_3N_4 QDs

was removed from surface, Rct was smaller than Rct of MIP/g-C_3N_4QDs/GCE without elution.

To demonstrate the difference between impressed and unprinted electrodes, differential pulse voltammograms (DPVs) were also registered. For the first time, only the buffer solution was used with MIP/g-C_3N_4QDs/GCE (curve an of Fig. 5A); and the obvious signal was not received without the analyte molecules.

Nonetheless, MIP/g-C_3N_4QDs/GCE demonstrated an obvious current signal at + 0.25 V in the presence of 10.0 nM AMP (curve c of Fig. 5A). NIP/g-C_3N_4QDs/GCE displayed smaller current signal (curve b of Fig. 5A). Therefore, in contrast with NIP/g-C_3N_4QDs/GCE, the MIP/g-C_3N_4QDs/GCE displayed greater imprinting selectivity. The MIP/g-C_3N_4QDs/GCE (curve c of Fig. 5B) showed the most effective sensor response according to received DPVs of various imprinted electrodes.

3.4 Optimization

3.4.1 pH effect

Due to its significant impact on sensor reaction, firstly, the pH effect was investigated. The current signals increased up to pH 7.5 based on the received DPVs from MIP/g-C_3N_4QD/GCE (Fig. 6a). However, the sensor signals dropped after a pH of 7.5. Therefore, the optimum pH was 7.5. An analysis of linear relationships was conducted between Ep and pH. The equations were achieved to be "$Epa = -0.0597pH + 0.674\ (R^2 = 0.9937)$" and "$Epc = -0.0613pH + 0.719\ (R^2 = 0.9991)$". The drops of − 59.7 and − 61.3 mV/pH showed that the electrochemical reaction involved two-protons and two-electron processes [45, 46].

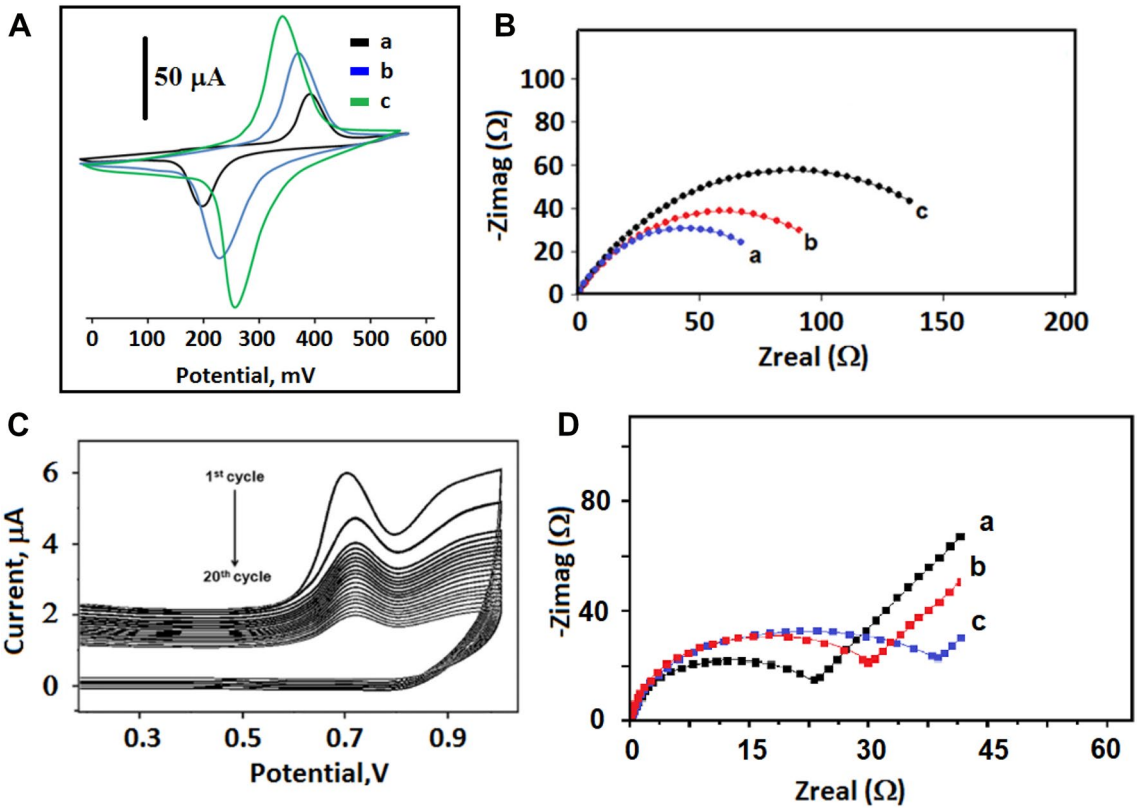

Fig. 4 **A** Cyclic voltammograms at (a) bare GCE, (b) g-C_3N_4/GCE, (c) g-C_3N_4QDs/GCE Scan rate: 100 mV s^{-1}; **B** EIS response at (a) g-C_3N_4QDs/GCE, (b) g-C_3N_4/GCE, (c) bare GCE (Frequency range is 100000–0.1 Hz, Wave amplitude 20 mV and formal potential: 0.155 V); In presence of 1.0 mM $[Fe(CN)_6]^{3-}$ containing 0.1 M KCl; **C** The electrochemical polymerization of 100 mM pyrrole containing 25.0 mM AMP on g-C_3N_4QDs/GCE (Scan rate: 100 mV s^{-1}); **D** EIS response at (a) g-C_3N_4QDs/GCE, (b) MIP/g-C_3N_4QDs/GCE after the removing of AMP, (c) MIP/g-C_3N_4QDs/GCE with AMP

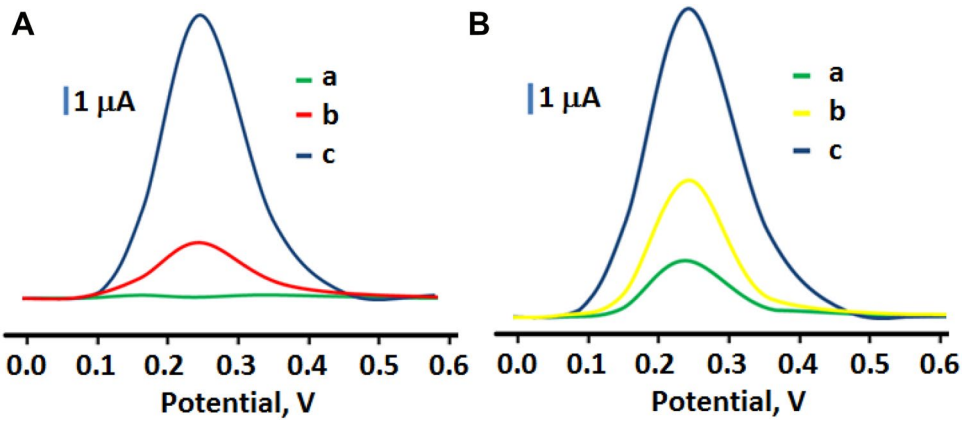

Fig. 5 **A** DPVs of MIP/g-C_3N_4QDs/GCE in presence of 0.1 M PBS (pH 7.5) (a), NIP/g-C_3N_4QDs/GCE in presence of 10.0 nM AMP (b), MIP/g-C_3N_4QDs/GCE in presence of 10.0 nM AMP (c) (frequency of 50 Hz, pulse amplitude of 20 mV, scan increment of 3 mV); **B** DPVs on imprinted electrodes in presence of 10.0 nM AMP (a) MIP/GCE; (b) MIP/g-C_3N_4/GCE; (c) MIP/g-C_3N_4QDs/GCE (frequency of 50 Hz, pulse amplitude of 20 mV, scan increment of 3 mV)

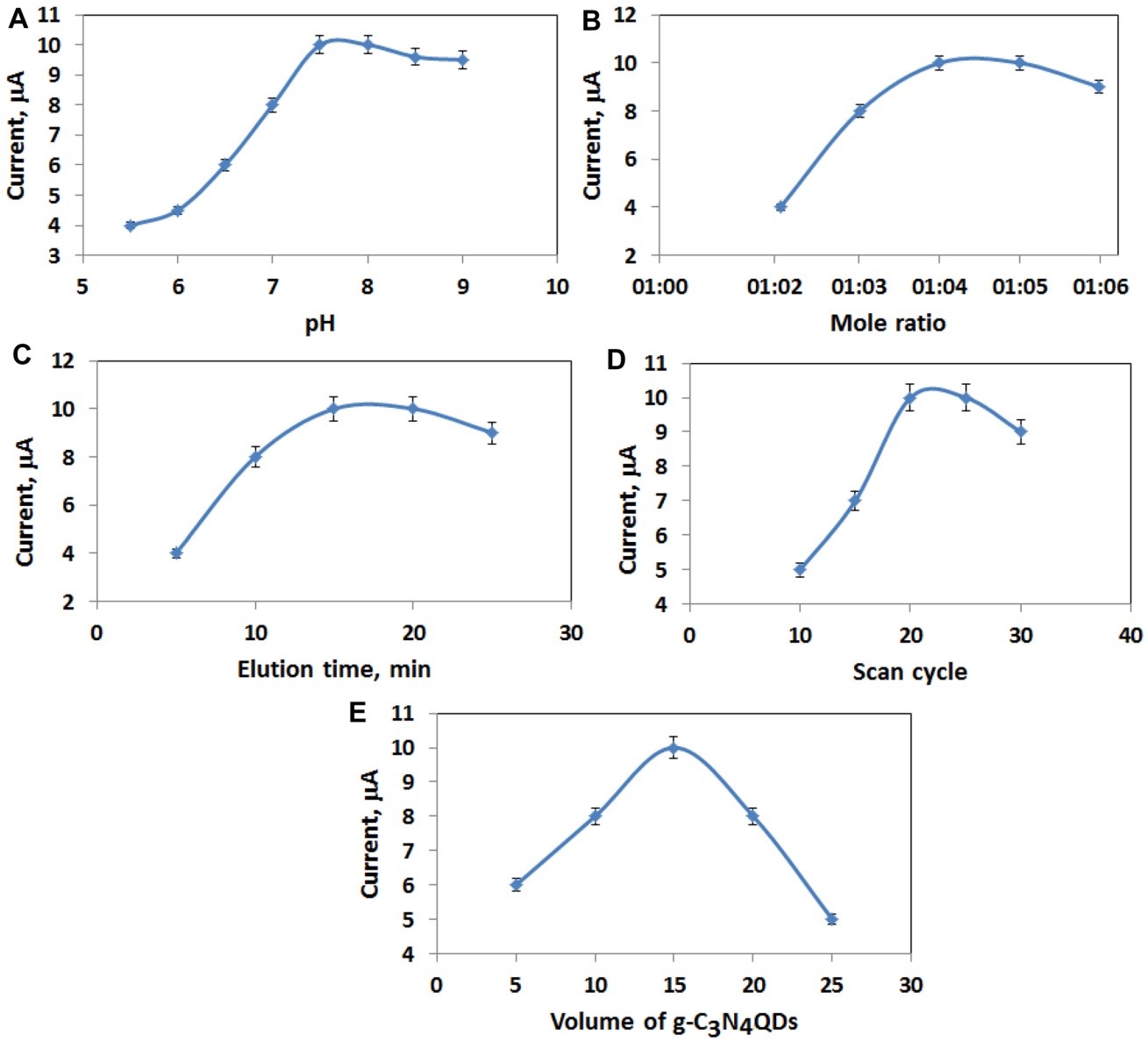

Fig. 6 Effect of **a** pH, **b** mole ratio, **c** elution time, **d** scan cycle, **e** quantum dots volume on DPVs (in the presence of 10.0 nM AMP) (n = 7) (frequency of 50 Hz, pulse amplitude of 20 mV, scan increment of 3 mV)

3.4.2 Mole ratio AMP molecule to pyrrole effect

To optimize the response on the sensors, monomer mole ratios and analyte molecules were constantly modified (Fig. 6b). Optimal and symmetric peaks were detected in a mixture of 100.0 mM monomer and 25.0 mM analyte. Up to 100.0 mM monomer, the number of target molecule belonging to binding sites increased. After 100.0 mM monomer, the optimal and symmetric peaks, in particular, deformed resulting from non-specific interactions on the electrode surface.

3.4.3 Effect of removal time

Throughout the present study, the elution time effect was investigated with the aim of ensuring complete molecular removal from the electrode surface (Fig. 6c). The response of the sensor was observed to last for more than 15 min. The sensor signals (µA) are either stayed constant or decreased slightly after 15 min. The optimal removal time was, therefore, chosen to be 15 min.

3.4.4 Effect of the scan cycle

The scan period generally affected the sensitivity and efficiency of the sensor. Various scans were tried so as to achieve specific interactions between monomer and analyte, in the current study (Fig. 6d). The optimal highest and signals were achieved by 20th scan cycle in the presence of 10.0 nM AMP as shown by DPVs in the presence of 10.0 nM AMP.

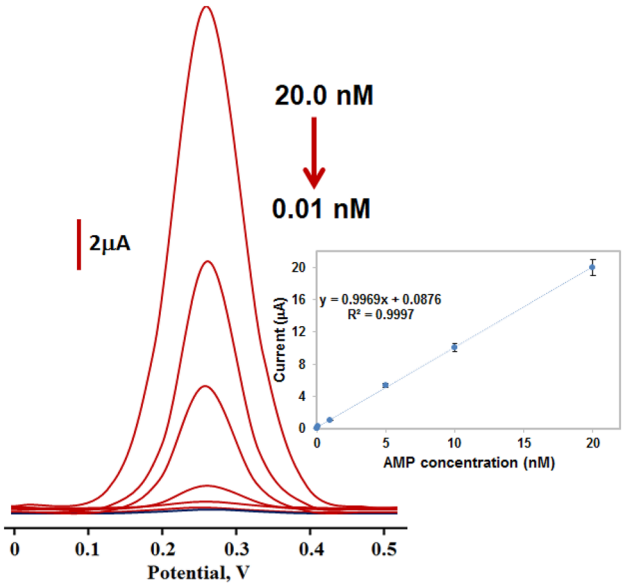

Fig. 7 Effect of concentration on the current signals with DPVs: Inset: Calibration curve of AMP concentrations at MIP/g-C_3N_4QDs/GCE in pH 7.5 of PBS (from 1.0×10^{-11} to 2.0×10^{-8} M AMP) (frequency of 50 Hz, pulse amplitude of 20 mV, scan increment of 3 mV)

3.4.5 Quantum dots volume effect

The various amounts (from 5 to 25 µL) of g-C_3N_4QDs were diminished upon clean surface for appropriate fabrication of sensor. At 15 µL of dispersion, an optimal sensor response was observed. After the dispersion of 15 µL, however, a decrease of the signal was observed, which was attributed to thicker nanolayers that generate reduced charge transfer (Fig. 6e).

3.5 Linearity range

As presents in Fig. 7, there was a linear relationship between the MIP/g-C_3N_4QDs/GCE signals and AMP values. The calibration equation was y (µA) = 0.9969x (nM) + 0.0876. 1.0×10^{-11} M and 2.0×10^{-12} M were found as quantification limit (LOQ) and LOD. The comparisons in linear range and LOD was also displayed in Table 1. MIP/g-C_3N_4QDs/GCE indicated higher sensitive analyses with high selectivity.

Table 2 The recovery of AMP (n = 6)

Sample	Added AMP (nM)	Found AMP (nM)	Recovery (%)
Paracetamol tablet	–	2.17 ± 0.004	–
	1.00	3.18 ± 0.005	100.31 ± 1.0
	3.00	5.16 ± 0.003	99.81 ± 0.8
	5.00	7.16 ± 0.006	99.86 ± 0.5

Table 1 Comparison of the developed sensor with the other electrochemical methods

Material	Linear range (M)	LOD (M)	Refs.
Zn/Ni-ZIF-8–800	8.00×10^{-8}–8.00×10^{-5}	2.90×10^{-8}	[47]
MXene/SPE	2.50×10^{-5}–2.0×10^{-3}	4.80×10^{-8}	[48]
$MnFe_2O_4$/ PANI	6.30×10^{-6}–5.00×10^{-3}	2.23×10^{-7}	[49]
La^{3+}-CuO/MWCNTs	5.00×10^{-7}–9.00×10^{-3}	1.40×10^{-8}	[50]
MWCNTs/NF	9.90×10^{-6}–7.41×10^{-5}	5.20×10^{-8}	[51]
Au/NPCs	1.20×10^{-5}–9.51×10^{-4}	4.94×10^{-8}	[52]
Nd_{OX}-SWCNT	1.00×10^{-7}–9.50×10^{-6}	5.00×10^{-8}	[53]
FIA	1.30×10^{-4}–9.00×10^{-5}	1.10×10^{-6}	[54]
MWCNT/ZnO/AuNPs	5.00×10^{-8}–2.00×10^{-5}	9.00×10^{-9}	[55]
Pd NPs/POM/NHCSs	2.00×10^{-8}–6.30×10^{-7}	3.00×10^{-9}	[56]
MIP/g-C_3N_4QDs	1.00×10^{-11}–2.00×10^{-8}	2.00×10^{-12}	This study

MXene/SPE: Sreen-printed electrode was modified by MXene; $MnFe_2O_4$/PANI: manganese ferrite/polyaniline; La^{3+}-CuO/MWCNTs: lanthanum-doped fern-like CuO nanoleaves/multi-walled carbon nanotubes; MWCNTs/NF: multi-walled carbon nanotubes/Nafion; Au/NPCs: Au-embedded nanostructured porous carbon; Nd_{OX}-SWCNT: Nd_2O_3-single-walled carbon nanotubes; FIA: flow injection analysis; MWCNT/ZnO/AuNPs: multi-walled carbon nano-tube/zinc oxide/gold nanoparticles; Pd NPs/POM/NHCSs: Pd/polyoxometalate/nitrogen-doping hollow carbon spheres

3.6 Recovery

Initially, recovery tests (Table 2) showing the selectivity of the molecular imprinted sensor like graphitic carbon nitride quantum dots were performed. The close values to 100.00 percent showed that matrix presence in the paracetamol tablet could not have an impact on selective analysis of AMP on MIP/g-C_3N_4QDs/GCE. Furthermore, for the selectivity study of AMP in real samples, the standard addition method was utilized. The calibration equation of standard addition method was defined to be y (μA) = 0.9940x (nM) + 0.247. The slopes of the standard addition method and the method of normal calibration were almost the same. Hence, AMP could, therefore, be selectively detected without any interference. Additionally, the LC–MS/MS approach was benefitted for comparison determining MIP/g-C_3N_4QDs/GCE validity [57]. Table 3 displays the analytical findings in paracetamol tablet samples for AMP detection (Added AMP = 5.16 nM). No substantial difference between MIP/g-C_3N_4QDs/GCE and LC–MS/MS was detected according to Wilcoxon's test (Tcalculated > Ttabulated, $p > 0.05$).

Table 3 Comparative analysis of findings obtained through AMP imprinted g-C_3N_4QDs/GCE and LC–MS/MS methods for the assessment of AMP (n = 6) (Added AMP = 5.16 nM)

Sample	Found AMP	
	MIP/g-C_3N_4QDs/GCE	LC–MS/MS
Paracetamol tablet (nM)	5.16 ± 0.003	5.14 ± 0.002
SD	0.007	0.005
RSD	0.14	0.09

RSD % Relative Standard Deviation, *SD* Standard Deviation $\overline{X}$ Mean ± Standard Error

3.7 Selectivity, stability, repeatability, reproducibility, and reusability

In the presence of AMP, LPA, DPA, LAA, LA, GLU, and AA, the selectivity experiments were tested for other selectivity measures. Therefore, seven separate solutions (10.0 nM AMP, LPA, DPA, LAA, LA, GLU, and AA in the presence of 0,1 M PBS, pH 7,5) were prepared. Following that, each of the solutions interacted with MIP/g-C_3N_4QDs/GCE separately. As shown in Fig. 8a, the highest sensor signals ($\Delta I = 10.00$ μA) were found with 10.0 nM AMP. In addition, MIP/g-C_3N_4QDs/GCE observed low non-specific sensor signals for LPA ($\Delta I = 2.50$ μA), LAA ($\Delta I = 1.25$ μA), DPA ($\Delta I = 1.70$ μA), GLU ($\Delta I = 0.80$ μA), LA ($\Delta I = 2.00$ μA), and AA ($\Delta I = 0.40$ μA). The structural and physicochemical parameters between AMP and

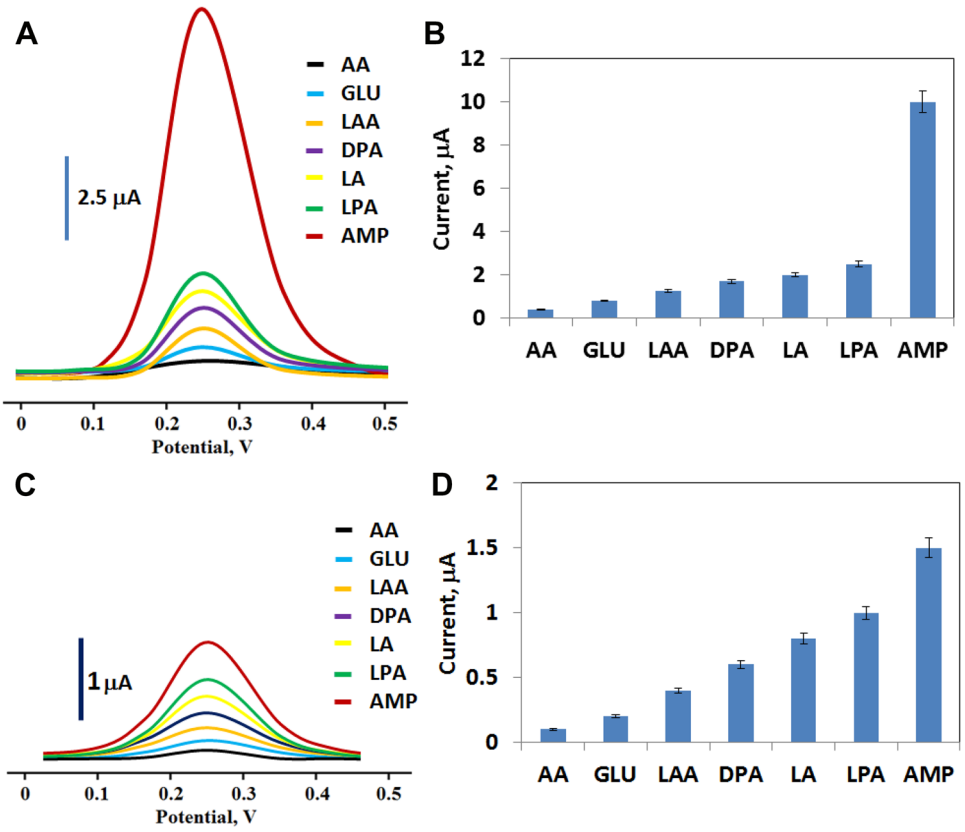

Fig. 8 **a** DPVs relating to 10.0 nM AMP, LPA, DPA, LAA, LA, GLU and AA on MIP/g-C_3N_4QDs/GCE (frequency of 50 Hz, pulse amplitude of 20 mV, scan increment of 3 mV); **b** Histogram of 10.0 nM AMP, LPA, DPA, LAA, LA, GLU and AA on MIP/g-C_3N_4QDs/GCE; **c** DPVs relating to 10.0 nM AMP, LPA, DPA, LAA, LA, GLU and AA on NIP/g-C_3N_4QDs/GCE (frequency of 50 Hz, pulse amplitude of 20 mV, scan increment of 3 mV); **d** Histogram of 10.0 nM AMP, LPA, DPA, LAA, LA, GLU and AA on NIP/g-C_3N_4QDs/GCE

Table 4 The selectivity coefficients (k) and relative selectivity coefficients (k′) values of MIP/g-C_3N_4QDs/GCE and NIP/g-C_3N_4QDs/GCE

	MIP		NIP		k′
	ΔI	k	ΔI	k	
AMP	10.00	–	1.50	–	–
LPA	2.50	4.00	1.00	1.50	2.67
DPA	1.70	5.80	0.60	2.50	2.32
LAA	1.25	8.00	0.40	3.75	2.13
LA	2.00	5.00	0.80	1.88	2.66
GLU	0.80	12.50	0.20	7.50	1.67
AA	0.40	25.00	0.10	15.00	1.67

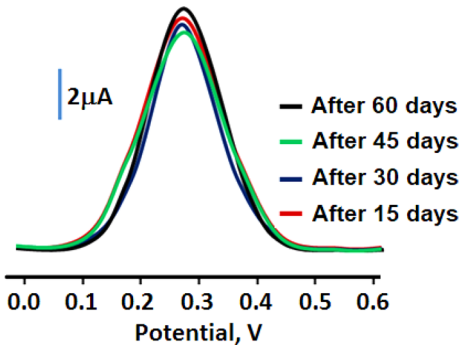

Fig. 9 Inter-day measurements for stability of one imprinted electrode (MIP/g-C_3N_4QDs/GCE) in presence of 10.0 nM AMP (frequency of 50 Hz, pulse amplitude of 20 mV, scan increment of 3 mV)

interfering agents were responsible for these fewer sensor signals. In comparison with LPA, DPA, LAA, LA, GLU, and AA, MIP/g-C_3N_4QDs/GCE was 4.00, 5.80, 8.00, 5.00, 12.50, and 25.00 times more selective towards AMP. The high sensor selectivity was thus confirmed, and an appropriate error interference analysis was accomplished (Fig. 8b and Table 4). Furthermore, the imprinting specificity was tested by means of NIP/g-C_3N_4QDs/GCE. The sensor signals and voltammograms were presented on Fig. 8c and Table 4, respectively. Figure 8d revealed the histogram of sensor signals on NIP/g-C_3N_4QDs/GCE. The NIP/g-C_3N_4QDs/GCE selectivity coefficients with LPA, DPA, LAA, GLU, and AA were 1.50, 2.50, 3.75, 1.88, 7.50, and 15.00, respectively. The relative selectivity constants meant that in contrast to LPA, DPA, LAA, GLU, and AA, the selectivity of MIP/ g-C3N4QDs/GCE was 2.67, 2.32, 2.13, 2.66, 1.67, and 1.77 times more selective.

For MIP/g-C_3N_4QDs/GCE stability, voltammograms were reported for 10.0 nM AMP during 60 days, and signals (10.0 μA) with 0.22% of relative standard deviation (RSD) were observed. The highly stable sensor was, therefore, prepared (Fig. 9).

60 Voltammograms were registered for repeatability of the MIP/g-C_3N_4QDs/GCE, and the replicable responses at + 0.25 V with 0.17% of RSD were recorded. MIP/g-C_3N_4QDs/GCE reproducibility and reusability tests were assessed, as well. In presence of 10.0 nM AMP, the reproducibility test was performed using 20 various sensors. The same procedure was utilized to manufacture these sensors independently. For sensor signals, the value of RSD is 0.29%. This low RSD value showed the reliability of the sensor production process. As a final step, the MIP/g-C_3N_4QDs/GCE reusability was tested. At least 30 times (0.20%), only one sensor could be used.

4 Conclusion

The new molecular-imprinted sensor was developed in the current study and it was utilized in pharmaceutical samples for acetaminophen recognition. The selective and porous sensor was successfully developed for AMP detection through molecular imprinting technique in accordance with the characterization results. In this respect, the performances as the LOD (2.0×10^{-12} M), linearity range (1.0×10^{-11}–2.0×10^{-8} M) and the sensor properties such as selectivity, stability, repeatability, reproducibility and reusability, were examined following the characterization of the sensor. The present study confirmed the validity of the sensor. Accordingly, the sensor can be suggested to appropriate for using in pharmaceutical samples for acetaminophen analysis.

References

1. Yang L, Yu LE, Ray MB (2008) Degradation of paracetamol in aqueous solutions by TiO2 photocatalysis. Water Res 42:3480–3488. https://doi.org/10.1016/j.watres.2008.04.023
2. Wu S, Zhang L, Chen J (2012) Paracetamol in the environment and its degradation by microorganisms. Appl Microbiol Biotechnol 96:875–884. https://doi.org/10.1007/s00253-012-4414-4
3. Ali AM, Rønning HT, Alarif W et al (2017) Occurrence of pharmaceuticals and personal care products in effluent-dominated Saudi Arabian coastal waters of the Red Sea. Chemosphere 175:505–513. https://doi.org/10.1016/j.chemosphere.2017.02.095
4. Morelli B (1989) Spectrophotometric determination of paracetamol in pure form and in tablets. J Pharm Biomed Anal 7:577–584. https://doi.org/10.1016/0731-7085(89)80223-7
5. Easwaramoorthy D, Yu Y-C, Huang H-J (2001) Chemiluminescence detection of paracetamol by a luminol-permanganate based reaction. Anal Chim Acta 439:95–100. https://doi.org/10.1016/S0003-2670(01)00968-0
6. Zhu W, Huang H, Gao X, Ma H (2014) Electrochemical behavior and voltammetric determination of acetaminophen based on glassy carbon electrodes modified with poly(4-aminobenzoic acid)/electrochemically reduced graphene oxide composite films. Mater Sci Eng C 45:21–28. https://doi.org/10.1016/j.msec.2014.08.067

7. Yola ML, Atar N (2018) Gold nanoparticles/two-dimensional (2D) hexagonal boron nitride nanosheets ıncluding diethylstilbestrol ımprinted polymer: electrochemical detection in urine samples and validation. https://doi.org/10.1149/2.0421814jes
8. Yola ML, Atar N (2017) A highly efficient nanomaterial with molecular imprinting polymer: Carbon nitride nanotubes decorated with graphene quantum dots for sensitive electrochemical determination of chlorpyrifos
9. Atar N, Yola ML (2021) A novel QCM immunosensor development based on gold nanoparticles functionalized sulfur-doped graphene quantum dot and h-ZnS-CdS NC for Interleukin-6 detection. Anal Chim Acta 1148:338202. https://doi.org/10.1016/j.aca.2021.338202
10. Chen X, He X, Gao J et al (2019) Three-dimensional porous Ni, N-codoped C networks for highly sensitive and selective nonenzymatic glucose sensing. Sens Actuators B Chem 299:126945. https://doi.org/10.1016/j.snb.2019.126945
11. Ding B, Ong W-J, Jiang J et al (2020) Uncovering the electrochemical mechanisms for hydrogen evolution reaction of heteroatom doped M2C MXene (M = Ti, Mo). Appl Surf Sci 500:143987. https://doi.org/10.1016/j.apsusc.2019.143987
12. Jiang J, Li N, Zou J et al (2019) Synergistic additive-mediated CVD growth and chemical modification of 2D materials. Chem Soc Rev 48:4639–4654. https://doi.org/10.1039/C9CS00348G
13. Jiang J, Ou-yang L, Zhu L et al (2014) Dependence of electronic structure of g-C3N4 on the layer number of its nanosheets: a study by Raman spectroscopy coupled with first-principles calculations. Carbon 80:213–221. https://doi.org/10.1016/j.carbon.2014.08.059
14. Jiang J, Zhu L, Zou J et al (2015) Micro/nano-structured graphitic carbon nitride–Ag nanoparticle hybrids as surface-enhanced Raman scattering substrates with much improved long-term stability. Carbon 87:193–205. https://doi.org/10.1016/j.carbon.2015.02.025
15. Li B, Wu Y, Li N et al (2020) Single-metal atoms supported on MBenes for robust electrochemical hydrogen evolution. ACS Appl Mater Interfaces 12:9261–9267. https://doi.org/10.1021/acsami.9b20552
16. Medetalibeyoglu H, Kotan G, Atar N, Yola ML (2020) A novel and ultrasensitive sandwich-type electrochemical immunosensor based on delaminated MXene@AuNPs as signal amplification for prostate specific antigen (PSA) detection and immunosensor validation. Talanta 220:121403. https://doi.org/10.1016/j.talanta.2020.121403
17. Sun Y, Jiang J, Cao Y et al (2018) Facile fabrication of g-C3N4/ZnS/CuS heterojunctions with enhanced photocatalytic performances and photoconduction. Mater Lett 212:288–291. https://doi.org/10.1016/j.matlet.2017.10.111
18. Yola ML, Atar N (2020) Amperometric galectin-3 immunosensor-based gold nanoparticle-functionalized graphitic carbon nitride nanosheets and core–shell Ti-MOF@COFs composites. Nanoscale 12:19824–19832. https://doi.org/10.1039/D0NR05614F
19. Zou J, Cao Y, Sun Y et al (2018) A comparative study of the photoconduction, photocatalytic and electrocatalytic performance of g-C 3 N 4 /ZnS/CuS heterojunctions with different morphologies. Catal Lett 148:3342–3348. https://doi.org/10.1007/s10562-018-2543-9
20. Zou J, Deng W, Jiang J et al (2020) Built-in electric field-assisted step-scheme heterojunction of carbon nitride-copper oxide for highly selective electrochemical detection of p-nonylphenol. Electrochim Acta 354:136658. https://doi.org/10.1016/j.electacta.2020.136658
21. Zou J, Mao D, Wee ATS, Jiang J (2019) Micro/nano-structured ultrathin g-C3N4/Ag nanoparticle hybrids as efficient electrochemical biosensors for l-tyrosine. Appl Surf Sci 467–468:608–618. https://doi.org/10.1016/j.apsusc.2018.10.187
22. Zou J, Wu S, Liu Y et al (2018) An ultra-sensitive electrochemical sensor based on 2D g-C3N4/CuO nanocomposites for dopamine detection. Carbon 130:652–663. https://doi.org/10.1016/j.carbon.2018.01.008
23. Wang Y, Wang X, Antonietti M (2012) Polymeric graphitic carbon nitride as a heterogeneous organocatalyst: from photochemistry to multipurpose catalysis to sustainable chemistry. Angew Chem Int Ed 51:68–89. https://doi.org/10.1002/anie.201101182
24. Cao S, Low J, Yu J, Jaroniec M (2015) Polymeric photocatalysts based on graphitic carbon nitride. Adv Mater 27:2150–2176. https://doi.org/10.1002/adma.201500033
25. Gong Y, Li M, Li H, Wang Y (2015) Graphitic carbon nitride polymers: promising catalysts or catalyst supports for heterogeneous oxidation and hydrogenation. Green Chem 17:715–736. https://doi.org/10.1039/C4GC01847H
26. Hashemi SH, Kaykhaii M, Jamali Keikha A, Naruie N (2020) Application of molecularly imprinted polymer pipette tip microsolid phase extraction of nalidixic acid and acetaminophen from pills and seawater samples and their determination by spectrophotometry. Chem Pap 74:4009–4023. https://doi.org/10.1007/s11696-020-01215-0
27. Xu Y-H, Xu G, Sun M-Y, Wang K (2020) Low-temperature solvothermal–calcination preparation and enhanced photocatalytic performance of polymeric graphitic carbon nitride with disordered–ordered hybrid plane. Chem Pap 74:4067–4074. https://doi.org/10.1007/s11696-020-01227-w
28. Zhang N, Wen L, Yan J, Liu Y (2020) Dye-sensitized graphitic carbon nitride (g-C3N4) for photocatalysis: a brief review. Chem Pap 74:389–406. https://doi.org/10.1007/s11696-019-00929-0
29. Gupta N, Gupta SM, Sharma SK (2019) Carbon nanotubes: synthesis, properties and engineering applications. Carbon Lett 29:419–447. https://doi.org/10.1007/s42823-019-00068-2
30. Feng S, Pei F, Wu Y et al (2021) A ratiometric fluorescent sensor based on g-CNQDs@Zn-MOF for the sensitive detection of riboflavin via FRET. Spectrochim Acta A Mol Biomol Spectrosc 246:119004. https://doi.org/10.1016/j.saa.2020.119004
31. Lv J, Feng S, Ding Y et al (2019) A high-performance fluorescent probe for dopamine detection based on g-C3N4 nanofibers. Spectrochim Acta A Mol Biomol Spectrosc 212:300–307. https://doi.org/10.1016/j.saa.2019.01.010
32. Lv X, Pei F, Feng S et al (2020) Facile synthesis of protonated carbon nitride/Ti3C2Tx nanocomposite for simultaneous detection of Pb2$\mathplus$ and Cd2$\mathplus$. J Electrochem Soc 167:067509. https://doi.org/10.1149/1945-7111/ab7e22
33. Wu S-R, Liu J-B, Wang H, Yan H (2019) NiO@ graphite carbon nanocomposites derived from Ni-MOFs as supercapacitor electrodes. Ionics 25:1–8. https://doi.org/10.1007/s11581-018-2812-z
34. Yola ML, Eren T, Atar N (2016) A Molecular Imprinted Voltammetric Sensor Based on Carbon Nitride Nanotubes: Application to Determination of Melamine. J Electrochem Soc 163:B588. https://doi.org/10.1149/2.0311613jes
35. Yola ML, Atar N (2017) A highly efficient nanomaterial with molecular imprinting polymer: carbon nitride nanotubes decorated with graphene quantum dots for sensitive electrochemical determination of chlorpyrifos. J Electrochem Soc 164:B223. https://doi.org/10.1149/2.1411706jes
36. Yola ML, Göde C, Atar N (2017) Molecular imprinting polymer with polyoxometalate/carbon nitride nanotubes for electrochemical recognition of bilirubin. Electrochim Acta 246:135–140. https://doi.org/10.1016/j.electacta.2017.06.053
37. Chen X, Liu Q, Wu Q et al (2016) Incorporating graphitic carbon nitride (g-C3N4) quantum dots into bulk-heterojunction polymer solar cells leads to efficiency enhancement. Adv Funct Mater 26:1719–1728. https://doi.org/10.1002/adfm.201505321
38. Yokuş ÖA, Kardaş F, Akyıldırım O et al (2016) Sensitive voltammetric sensor based on polyoxometalate/reduced graphene oxide

nanomaterial: Application to the simultaneous determination of l-tyrosine and l-tryptophan. Sens Actuators B Chem 233:47–54. https://doi.org/10.1016/j.snb.2016.04.050
39. Yola ML, Atar N (2019) Development of cardiac troponin-I biosensor based on boron nitride quantum dots including molecularly imprinted polymer. Biosens Bioelectron 126:418–424. https://doi.org/10.1016/j.bios.2018.11.016
40. Arancibia V, Penagos-Llanos J, Nagles E et al (2019) Development of a microcomposite with single-walled carbon nanotubes and Nd2O3 for determination of paracetamol in pharmaceutical dosage by adsorptive voltammetry. J Pharm Anal 9:62–69. https://doi.org/10.1016/j.jpha.2018.11.005
41. Duan J, Chen S, Jaroniec M, Qiao SZ (2015) Porous C3N4 Nanolayers@N-Graphene films as catalyst electrodes for highly efficient hydrogen evolution. ACS Nano 9:931–940. https://doi.org/10.1021/nn506701x
42. Wang W, Yu JC, Shen Z et al (2014) g-C3N4 quantum dots: direct synthesis, upconversion properties and photocatalytic application. Chem Commun 50:10148–10150. https://doi.org/10.1039/C4CC02543A
43. Luo W-B, Chou S-L, Wang J-Z et al (2015) A metal-free, free-standing, macroporous graphene@g-C3N4 composite air electrode for high-energy lithium oxygen batteries. Small 11:2817–2824. https://doi.org/10.1002/smll.201403535
44. Hatamie A, Jalilian P, Rezvani E et al (2019) Fast and ultra-sensitive voltammetric detection of lead ions by two-dimensional graphitic carbon nitride (g-C3N4) nanolayers as glassy carbon electrode modifier. Measurement 134:679–687. https://doi.org/10.1016/j.measurement.2018.10.082
45. Alam AU, Qin Y, Howlader MMR et al (2018) Electrochemical sensing of acetaminophen using multi-walled carbon nanotube and β-cyclodextrin. Sens Actuators B Chem 254:896–909. https://doi.org/10.1016/j.snb.2017.07.127
46. Xu Y, Lei W, Su J et al (2018) A high-performance electrochemical sensor based on g-C3N4-E-PEDOT for the determination of acetaminophen. Electrochim Acta 259:994–1003. https://doi.org/10.1016/j.electacta.2017.11.034
47. Zhang W, Zong L, Liu S et al (2019) An electrochemical sensor based on electro-polymerization of caffeic acid and Zn/Ni-ZIF-8–800 on glassy carbon electrode for the sensitive detection of acetaminophen. Biosens Bioelectron 131:200–206. https://doi.org/10.1016/j.bios.2019.01.069
48. Wang C, Zhang N, Li Y et al (2019) Cobalt-based metal-organic frameworks as co-reaction accelerator for enhancing electrochemiluminescence behavior of N-(aminobutyl)-N-(ethylisoluminol) and ultrasensitive immunosensing of amyloid-β protein. Sens Actuators B Chem 291:319–328. https://doi.org/10.1016/j.snb.2019.04.097
49. Luk H-N, Peng H-Y, Han Y-W et al (2019) Detection of acetaminophen using cyclic voltammetry on $MnFe_2O_4$/polyaniline. J Chin Chem Soc 66:75–80. https://doi.org/10.1002/jccs.201800137
50. Foroughi MM, Jahani S, Hassani Nadiki H (2019) Lanthanum doped fern-like CuO nanoleaves/MWCNTs modified glassy carbon electrode for simultaneous determination of tramadol and acetaminophen. Sens Actuators B Chem 285:562–570. https://doi.org/10.1016/j.snb.2019.01.069
51. Kuyumcu Savan E (2019) Electrochemical determination of N-acetyl cysteine in the presence of acetaminophen at multi-walled carbon nanotubes and nafion modified sensor. Sens Actuators B Chem. https://doi.org/10.1016/j.snb.2018.11.092
52. Li F, Li R, Feng Y et al (2019) Facile synthesis of Au-embedded porous carbon from metal-organic frameworks and for sensitive detection of acetaminophen in pharmaceutical products. Mater Sci Eng C 95:78–85. https://doi.org/10.1016/j.msec.2018.10.074
53. Arancibia V, Penagos-Llanos J, Nagles E et al (2019) Development of a microcomposite with single-walled carbon nanotubes and Nd_2O_3 for determination of paracetamol in pharmaceutical dosage by adsorptive voltammetry. J Pharm Anal 9:62–69. https://doi.org/10.1016/j.jpha.2018.11.005
54. Frangu A, Pravcová K, Šilarová P et al (2019) Flow injection tyrosinase biosensor for direct determination of acetaminophen in human urine. Anal Bioanal Chem 411:2415–2424. https://doi.org/10.1007/s00216-019-01687-4
55. Kenarkob M, Pourghobadi Z (2019) Electrochemical sensor for acetaminophen based on a glassy carbon electrode modified with ZnO/Au nanoparticles on functionalized multi-walled carbon nano-tubes. Microchem J 146:1019–1025. https://doi.org/10.1016/j.microc.2019.02.038
56. Wang L, Meng T, Sun J et al (2019) Development of Pd/Polyoxometalate/nitrogen-doping hollow carbon spheres tricomponent nanohybrids: A selective electrochemical sensor for acetaminophen. Analytica Chimica Acta 1047:28–35. https://doi.org/10.1016/j.aca.2018.09.042
57. Cook SF, King AD, van den Anker JN, Wilkins DG (2015) Simultaneous quantification of acetaminophen and five acetaminophen metabolites in human plasma and urine by high-performance liquid chromatography–electrospray ionization–tandem mass spectrometry: method validation and application to a neonatal pharmacokinetic study. J Chromatogr B 1007:30–42. https://doi.org/10.1016/j.jchromb.2015.10.013